Regulating Reorganization Energy and Crystal Packing of Small-Molecule Donors Enables High Performance Binary All-Small-Molecule Organic Solar Cells with Slow Film Growth Rate

Tongle Xu,[a,1] Jie Lv,[b,1] Daming Zheng,[c,1] Zhenghui Luo,*[a] Min Hun Jee,[d] Guangliu Ran,[e] Zhanxiang Chen,[a] Zhongyan Huang,[a] Jiaqi Ren,[f] Yuxiang Li,[f] Cai'e Zhang,[a] Hanlin Hu,*[b] Thierry Pauporté,[c] Wenkai Zhang,*[e] Han Young Woo,*[d] and Chuluo Yang*[a]

[a]T. Xu, Z. Luo, Z. Chen, Z. Huang, C. Zhang, C. Yang
Shenzhen Key Laboratory of New Information Display and Storage Materials, College of Materials Science and Engineering, Shenzhen University, Shenzhen 518060, China. E-mail: zhhuiluo@szu.edu.cn; clyang@szu.edu.cn.

[b]J. Lv, H. Hu
Hoffmann Institute of Advanced Materials, Shenzhen Polytechnic, 7098 Liuxian Boulevard, Shenzhen 518055, China. E-mail: hanlinhu@szpt.edu.cn.

[c]D. Zheng, T. Pauporté
Chimie ParisTech, Université PSL, CNRS, Institut de Recherche de Chimie Paris (IRCP), UMR8247, 11 rue P. et M. Curie, F-75005, Paris, France.

[d]M. H. Jee, H. Y. Woo
Department of Chemistry, College of Science, Korea University, Seoul 136-713, Republic of Korea.
E-mail: hywoo@korea.ac.kr.

[e]G. Ran, W. Zhang
Department of Physics and Applied Optics Beijing Area Major Laboratory, Beijing Normal University, Beijing 100875, China. E-mail: wkzhang@bnu.edu.cn.

[f]J. Ren, Y. Li
School of Materials Science and Engineering, Xi'an University of Science and Technology, Xi'an 710054, China.

[1]T. Xu, J. Lv and D. Zheng contributed equally to this work.

Device Fabrication and Testing

Organic solar cells were prepared with regular structure: ITO/PEDOT:PSS/Active layer/ PDINN /Ag. Cleaning and retreatment of patterned ITO can be found elsewhere. PEDOT:PSS was diluted with the same volume of water, a thin layer of PEDOT:PSS (~20 nm) (Clevios Al 4083) was spin-coated onto the UV-treated substrates followed by thermal treatment on a hot plate at 150 °C for 15 min. Then, the HTL-covered samples were transferred into a nitrogen-filled glovebox for active layer deposition. The optimized overall concentration were 23 mg·ml^{-1} chloroform solution with feed ratio of 1.5:1 (w/w) for donors:Y6, respectively. Note: The as-prepared solutions were stirred at 40℃ temperature for 2 hours before being spin-coated. The active layers were spin-coated at an optimized speed of 2500 rpm for 30s, resulting in films of 100 to 120 nm in thickness. The active layers were then treated by CB solvent vapor annealing (SVA), after that, thermal treatment under different temperature was further conducted to optimize the active layer. Then, PDINN solution (2 mg/ml in isopropyl alcohol) was spin-coated on with 3000 rpm for 20s. Finally, these cells were transferred into a thermal evaporation chamber with a base pressure below 1×10^{-6} torr, and 100 nm of Ag was deposited with a deposition rate of 0.1-0.2 nm s^{-1}. The active area was 0.1 cm^2.

The current density-voltage (*J-V*) curves of devices were recorded under AM 1.5G illumination provided by an AAA class solar simulator (Enli Technology Co., Ltd. SS-X50R) calibrated by a silicon reference cell with KG1 filter (supported from Enli Tech. Co., Ltd., Taiwan). The external quantum efficiency (EQE) was measured by a certified incident photon to electron conversion (IPCE) equipment (QE-R) from Enli Technology Co., Lt. The light intensity at each wavelength was calibrated using a standard monocrystalline Si photovoltaic cell. The parasitic absorption was obtained from the transfer matrix model.

SCLC Mobility Measurements

Fitting the hole/electron-only diode dark current to the space charge limited current (SCLC) model can obtain the hole and electron mobility of the photosensitive active layer. The electron-only device structure was ITO/ZnO/ PDINN / Active layer / PDINN

/Ag, and the hole-only device structure was ITO/PEDOT:PSS/ Active layer /MoO_3/Ag. Using the following equation to estimate the electric-field dependent SCLC mobility:

$$J(V) = \frac{9}{8}\varepsilon_0\varepsilon_r\mu_0 exp\left(0.89\beta\sqrt{\frac{V - V_{bi}}{L}}\right)\frac{(V - V_{bi})^2}{L^3} \quad \textbf{(1)}$$

For the hole-only device structure, V_{bi} = 0 V (flat band pattern formed by PEDOT:PSS-MoO_3); For the electron-only device structure, V_{bi} = 0.5V was used following the protocol reported[1].

The functioning of a GD-OES equipment

In this technique, a low-pressure glow discharge plasma is generated. The sample material is polarized negatively and acts as a cathode. The cations in the plasma are accelerated toward the sample surface and kicks-out the surface atoms. This bombardment process, referred to as sputtering, ablates the sample in the direction perpendicular to the surface. The released analyte atoms are then promoted to an excited state by energy transfers from the plasma. While they return to their ground state, they emit light forming a glow. The emitted wavelengths are atom specific, and the sample composition is deduced from the real-time analysis by optical emission spec- troscopy of the emitted spectrum (Figure S7a).

Characterizations and Measurements

GD-OES analysis was performed using a HORIBA Jobin Yvon GD Profiler 2 apparatus. The instrument was equipped with a RF-generator (13.56 MHz), a standard HORIBA Jobin Yvon glow discharge source, cylindrical anodes with an inner diameter of 4 mm, and two optical spectrometers (one polychromatic and one monochromator) for rapid optical detection. The argon plasma was generated at an argon pressure of 420 Pa and the applied power was 10 W. The organic film was mounted on an O-ring on one side of the plasma chamber, which acts as a cathode. The analyzed perovskite film area was a disk 4 mm in diameter.

Materials

All reagents and solvents, unless otherwise specified, were purchased from Energy Chemical, Organtec.Ltd, JiangSu GE-Chem Biotech.,Ltd. All reagents were used as recieved without further purification. The intermediate **1b** is synthesized according to the previous literature report[2], **1a** is obtained in exactly the same way as **1b** and will not be repeated here. All reactions were heated by metal sand bath (WATTCAS, LAB-500, https://www.wattcas.com).

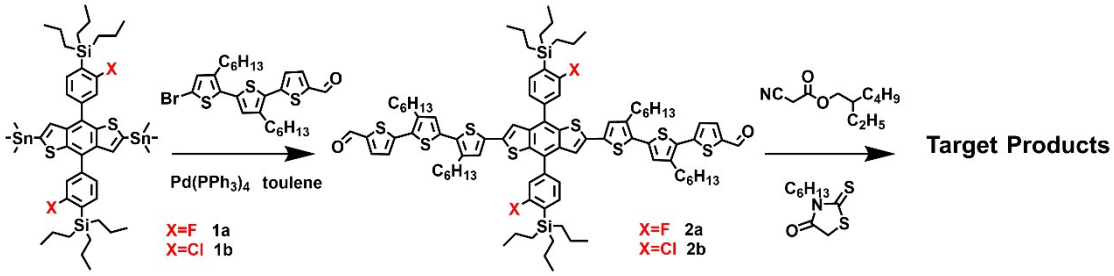

Scheme **S1**. Synthetic route of **T25**, **T26** and **T27**.

Synthesis of compound **2a**: In a pre-dried Schlenk tube, Compound **1a** (500 mg, 0.49 mmol), **2** (618 mg, 1.18 mmol) and $Pd(PPh_3)_4$ (50 mg) were dissolved with degassed toluene (30 mL). The mixture was heated at 130 °C for 24 h. The reaction mixture was allowed to cool down to room temperature, the organic layer was washed with brine, extracted with dichloromethane (3×40 mL), dried with anhydrous Na_2SO_4, and then concentrated under reduced pressure. The crude product was purified by column chromatography over silica gel using a mixture of chlorform and hexane (4:1) as the eluent to afford orange solid (543g, 70%). ^{1}H NMR (400 MHz, Chloroform-d) δ 9.88 (s, 2H), 7.71 (d, J = 4.0 Hz, 2H), 7.61 (dd, J = 7.5, 5.7 Hz, 2H), 7.48 (dd, J = 7.5, 1.5

Hz, 2H), 7.37-7.34 (dd, J = 7.5, 1.5 Hz, 2H), 7.34 (s, 2H), 7.23 (d, J = 4.0 Hz, 2H), 7.11 (s, 2H), 7.02 (s, 2H), 2.83-2.74 (m, 10H), 1.52-1.39 (m, 22H), 1.33-1.30 (m, 14H), 1.08-1.03 (m, 20H), 0.99-0.95 (m, 12H), 0.91-0.87 (m, 12H).^{13}C NMR (101 MHz, CDCl3) δ 182.53, 166.49, 146.00, 142.57, 142.24, 141.22, 137.83, 137.77, 136.88, 136.84, 135.85, 135.29, 130.56, 129.60, 129.15, 128.83, 128.62, 125.87, 124.67, 118.40, 115.60, 31.66, 30.40, 30.22, 29.80, 29.67, 29.27, 22.62, 18.63, 17.54, 15.42, 15.38, 14.10.

Synthesis of compound **2b**: The synthetic route is similar to that of compound **2a,** except for replacing **1a** with **1b**.^{1}H NMR (400 MHz, Chloroform-d) δ 9.89 (s, 2H), 7.70 (dd, J = 5.0, 2.8 Hz, 4H), 7.65 (d, J = 7.6 Hz, 2H), 7.56 (dd, J = 7.6, 1.6 Hz, 2H), 7.31 (s, 2H), 7.23 (d, J = 4.0 Hz, 2H), 7.12 (s, 2H), 7.02 (s, 2H), 2.83-2.74 (m, 8H), 1.75-1.60 (m, 10H), 1.54-1.40 (m, 22H), 1.34-1.30 (m, 14H), 1.08-1.02 (m, 32H), 0.91-0.86 (m, 12H).^{13}C NMR (101 MHz, CDCl3) δ 182.47, 145.97, 142.53, 142.20, 141.80, 141.16, 140.87, 137.87, 137.83, 137.45, 137.16, 136.89, 136.81, 135.83, 135.21, 130.61, 129.72, 129.60, 129.11, 128.63, 126.67, 125.82, 118.26, 31.67, 30.39, 30.22, 29.81, 29.69, 29.30, 22.64, 18.68, 17.69, 15.45, 14.12.

Synthesis of compound **T25:** Compound **2a** (140 mg, 0.09 mmol) and cyanoacetic acid esters (175 mg, 0.9 mmol) were added dissolved in chloroform (30 mL), then 2mL triethylamine added and resulting solution was heated to reflux and stirred overnight. The reaction mixture was concentrated under reduced pressure and by silica gel chromatography using a mixture of chlorform and hexane (4:1) as eluent to afford **T4** as black solid (160 mg, 92%).^{1}H NMR (400 MHz, Chloroform-d) δ 8.24 (s, 2H), 7.76

(d, J = 4.1 Hz, 2H), 7.62 (t, J = 6.7 Hz, 2H), 7.48 (d, J = 7.6 Hz, 2H), 7.38-7.33 (m, 4H), 7.23 (d, J = 3.9 Hz, 2H), 7.11 (d, J = 2.0 Hz, 2H), 7.02 (d, J = 2.0 Hz, 2H), 4.21 (d, J = 5.8 Hz, 4H), 2.83 (t, J = 7.9 Hz, 4H), 2.77 (t, J = 8.0 Hz, 4H), 1.73-1.64 (m, 12H), 1.42-1.30 (m, 40H), 1.09-1.03 (m, 22H), 0.98-0.87 (m, 42H). ^{13}C NMR (101 MHz, CDCl3) δ 166.48, 163.20, 146.25, 145.75, 142.95, 141.83, 141.33, 137.89, 137.84, 137.74, 136.88, 136.26, 135.38, 134.84, 130.55, 129.53, 129.28, 128.83, 128.63, 126.12, 124.66, 118.43, 115.99, 115.60, 97.68, 68.78, 38.80, 31.66, 30.34, 30.22, 29.99, 29.70, 29.27, 29.23, 28.93, 23.77, 22.97, 22.61, 18.63, 17.54, 15.42, 14.10, 14.06, 11.03. HRMS (m/z) $[M]^+$:1932.8549

Synthesis of compound **T26:** The synthetic route is similar to that of compound **T25,** except for replacing cyanoacetic acid esters with 3-hexylrhodanine.^{1}H NMR (600 MHz, Chloroform-d) δ 7.83 (s, 2H), 7.62 (dd, J = 7.5, 5.7 Hz, 2H), 7.48 (dd, J = 7.4, 1.5 Hz, 2H), 7.37-7.34 (m, 4H), 7.33 (s, 2H), 7.20 (d, J = 4.0 Hz, 2H), 7.10 (s, 2H), 7.01 (s, 2H), 4.09 (t, J = 7.7 Hz, 4H), 2.82-2.79 (t, J = 8.0 Hz, 4H), 2.76 (t, J = 8.0 Hz, 4H), 1.72-1.66 (m, 12H), 1.51-1.39 (m, 22H), 1.36-1.30 (m, 26H), 1.07-1.04 (m, 18H), 0.99-0.95 (m, 12H), 0.92-0.87 (m, 18H). ^{13}C NMR (151 MHz, Chloroform-d) δ 192.11, 168.49, 167.49, 166.89, 144.23, 141.93, 141.70, 141.65, 141.05, 137.81, 137.73, 137.08, 136.87, 136.67, 136.59, 135.49, 135.15, 134.66, 130.71, 129.79, 129.09, 128.75, 128.73, 128.60, 126.48, 124.96, 124.79, 124.69, 124.67, 124.58, 120.19, 118.31, 115.58, 115.39, 44.86, 31.74, 31.70, 31.37, 30.37, 30.30, 29.90, 29.75, 29.38, 29.34, 26.95, 26.50, 22.71, 22.67, 22.60, 22.57, 18.70, 17.58, 15.44, 15.43, 14.19, 14.18, 14.06. HRMS (m/z) $[M]^+$:1972.6907

Synthesis of compound **T27:** The synthetic route is similar to that of compound **T26,** except for replacing **2a** with **2b**. ^{1}H NMR (400 MHz, Chloroform-d) δ 7.82 (s, 2H), 7.70 (d, J = 1.6 Hz, 2H), 7.66 (d, J = 7.6 Hz, 2H), 7.56 (dd, J = 7.6, 1.6 Hz, 2H), 7.34 (d, J = 4.0 Hz, 2H), 7.29 (s, 2H), 7.19 (d, J = 4.0 Hz, 2H), 7.10 (s, 2H), 7.00 (s, 2H), 4.12-4.06 (t, J = 7.6 Hz, 4H), 2.82-2.73 (m, 8H), 1.73-1.65 (m, 12H), 1.51-1.42 (m, 18H), 1.36-1.30 (m, 26H), 1.09-1.01 (m, 32H), 0.93-0.85 (m, 20H). ^{13}C NMR (151 MHz, Chloroform-d) δ 192.13, 192.07, 167.50, 167.44, 144.23, 141.93, 141.88, 141.79, 141.06, 140.97, 140.87, 137.85, 137.79, 137.74, 137.43, 137.41, 137.16, 137.08, 137.00, 136.88, 136.86, 135.46, 135.45, 135.09, 135.02, 134.67, 134.62, 130.75, 129.80, 129.78, 129.74, 129.12, 129.01, 128.66, 128.61, 128.50, 128.44, 126.68, 126.50, 126.40, 126.36, 124.98, 124.92, 120.20, 120.11, 118.21, 44.87, 44.84, 31.76, 31.75, 31.71, 31.69, 31.37, 30.36, 30.30, 30.28, 29.92, 29.89, 29.79, 29.76, 29.74, 29.40, 29.37, 29.34, 26.95, 26.93, 26.50, 22.73, 22.71, 22.69, 22.68, 22.57, 18.73, 17.71, 15.45, 14.20, 14.07. MALDI-TOFMS (m/z) $[M]^{+}$:2008.1576

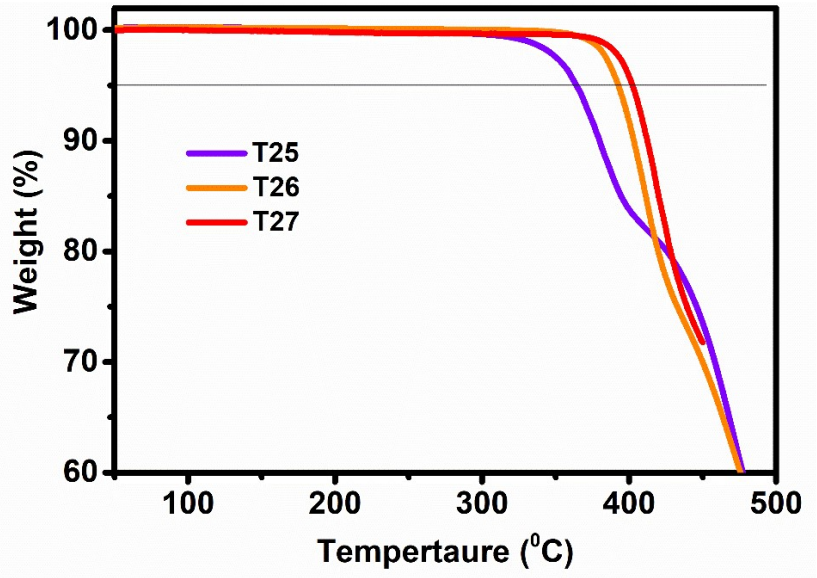

Figure S1. Thermogravimetric analysis (TGA) curve of the **T25**, **T26** and **T27.**

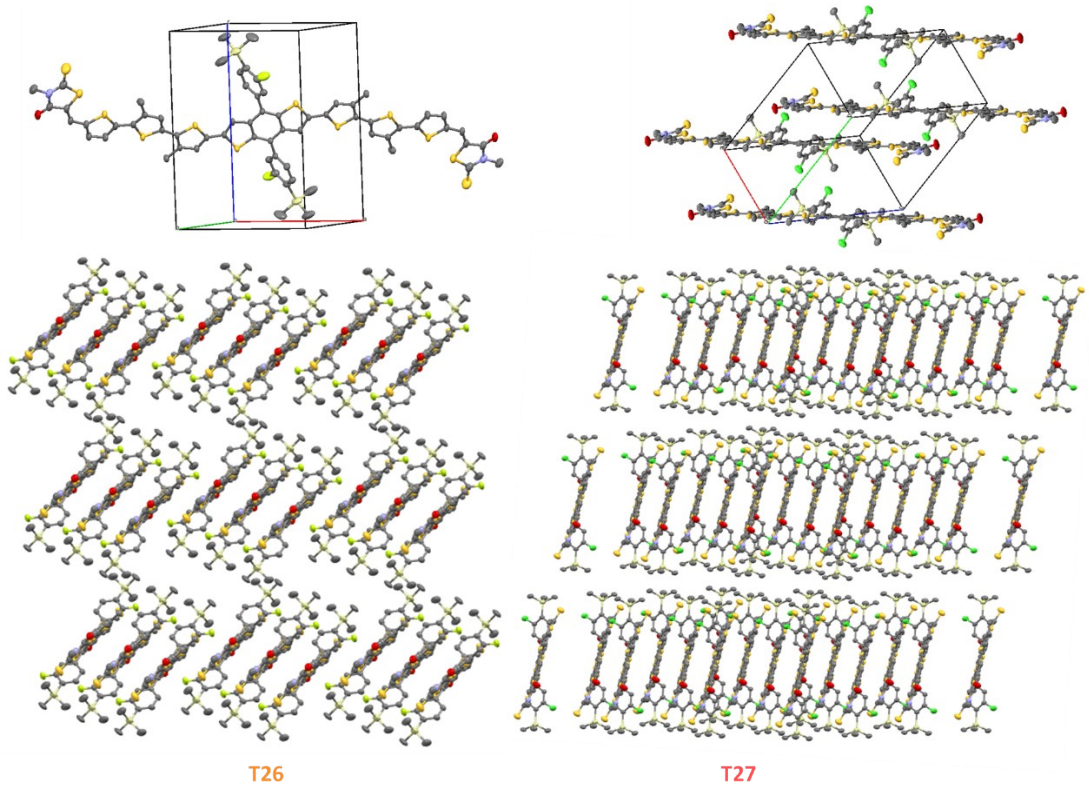

Figure S2. The packing images of **T26** and **T27** single crystals.

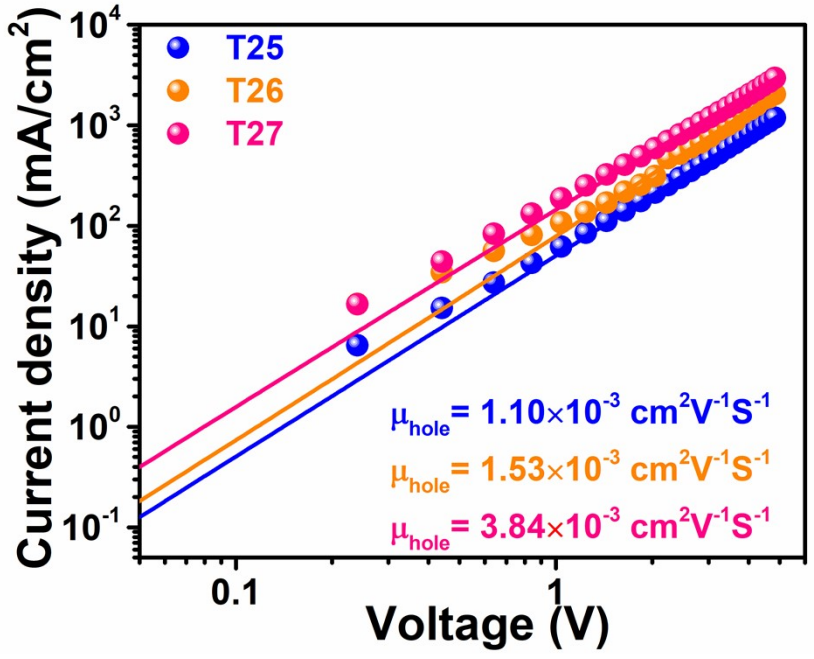

Figure S3. The neat film hole mobility of T25, T26 and T27

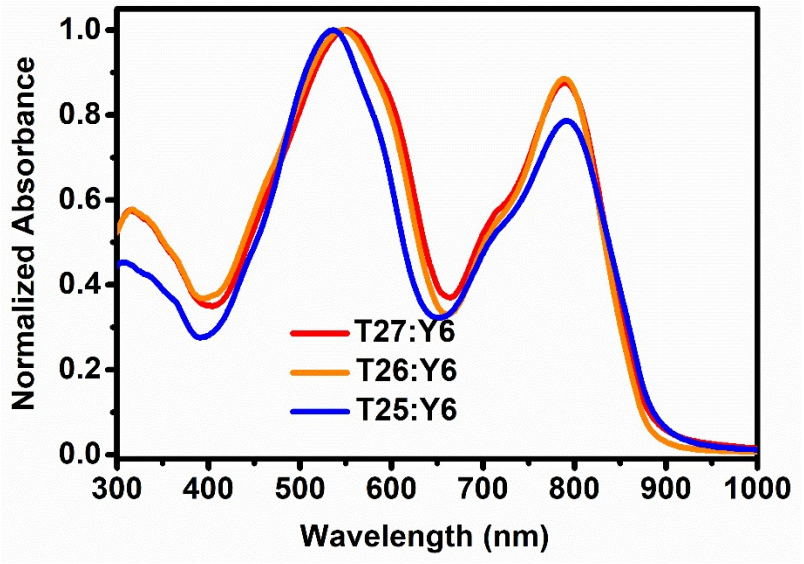

Figure S4. Absorption spectra of the blend films of **T25:Y6**, **T26:Y6** and **T27:Y6.**

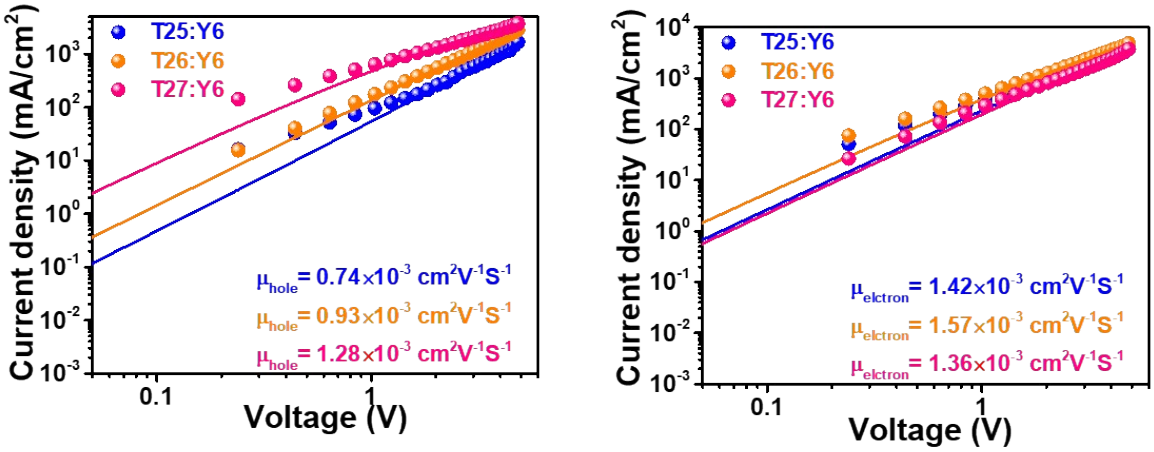

Figure S5. SCLC date for (a) electron-only and (b) hole-only devices fabricated by T25:Y6, T26:Y6 and T27:Y6 respectively.

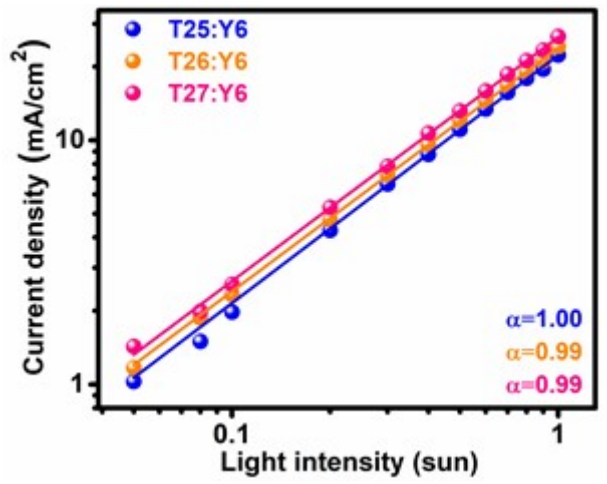

Figure S6. Jsc dependence on the light intensity

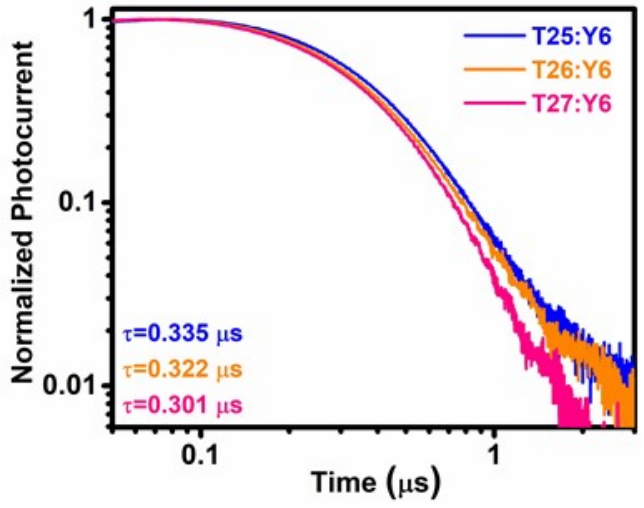

Figure S7. Transient photocurrent of the blends.

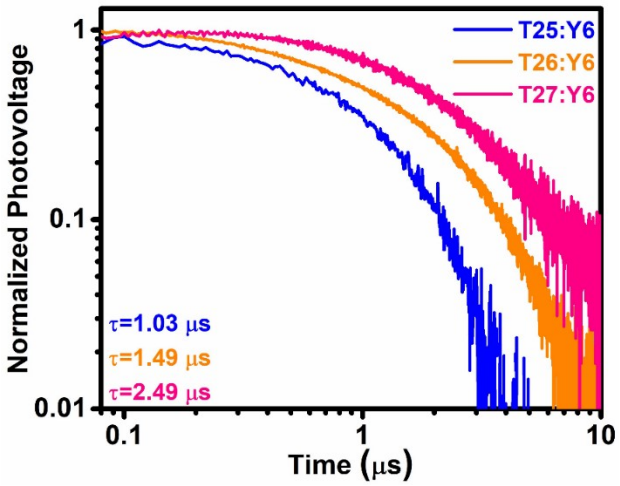

Figure S8. Transient photovoltage of the blends.

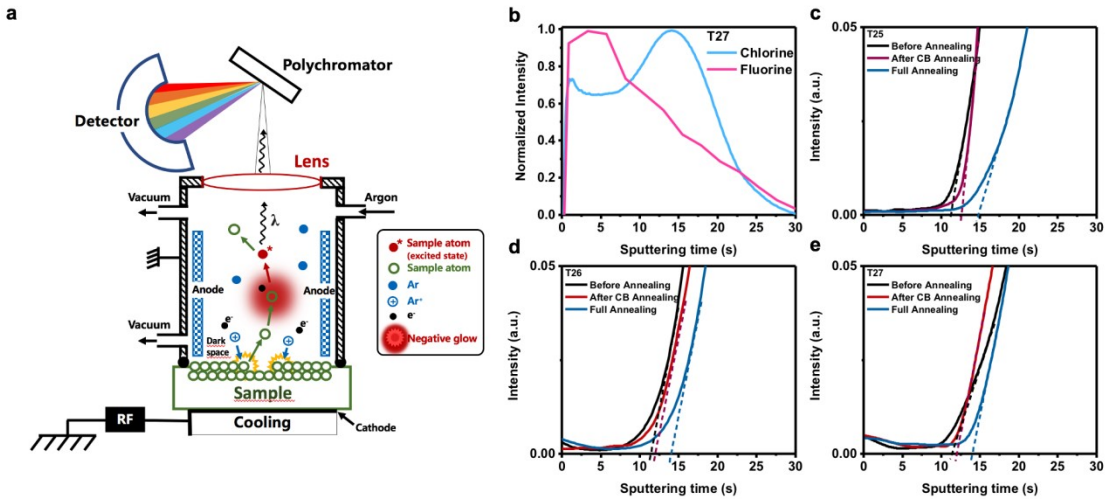

Figure S9. (a) Schematic of a GD-OES instrument working principle. (b) The GD-OES depth profile of the fully annealed organic layer of T27:Y6. (d-e) The GD-OES depth profiles of substrate of (b) T25:Y6, (c) T26:Y6, and (d) T27:Y6.

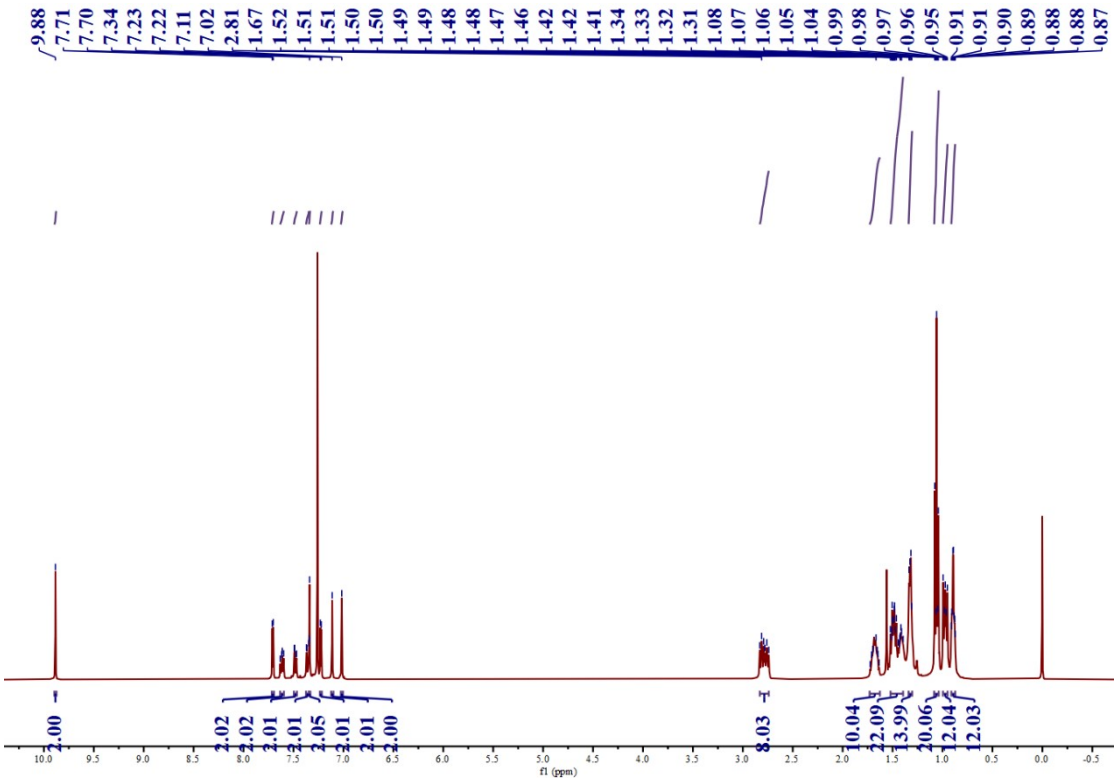

Figure S10. ^{1}H NMR spectrum of compound 2a in $CDCl_3$.

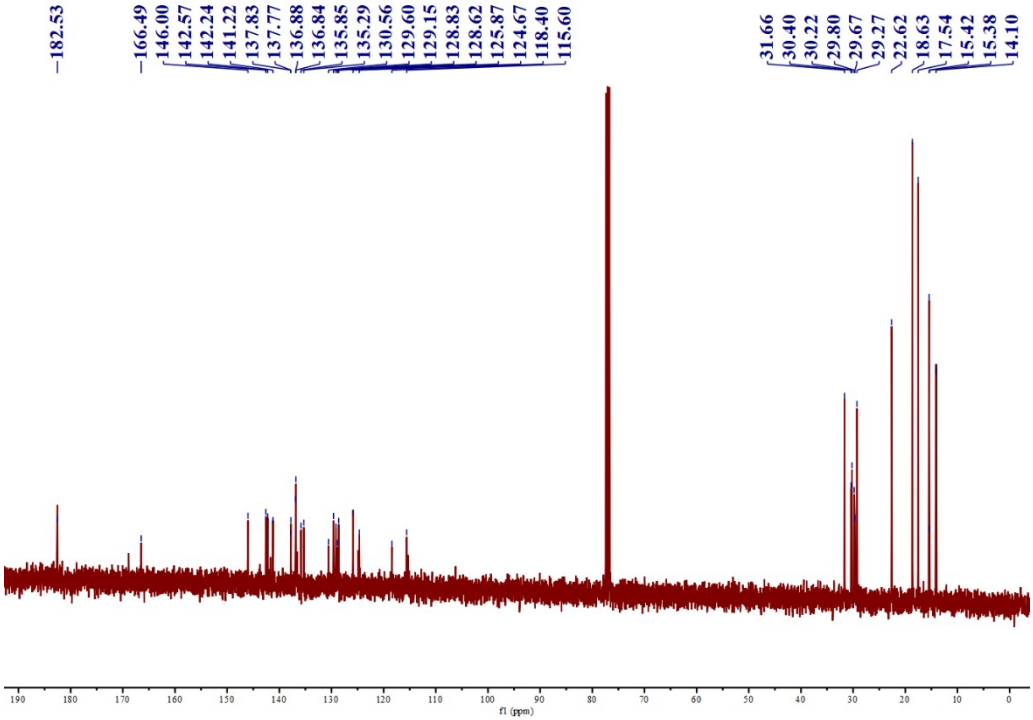

Figure S11. ^{13}C NMR spectrum of compound 2a in $CDCl_3$.

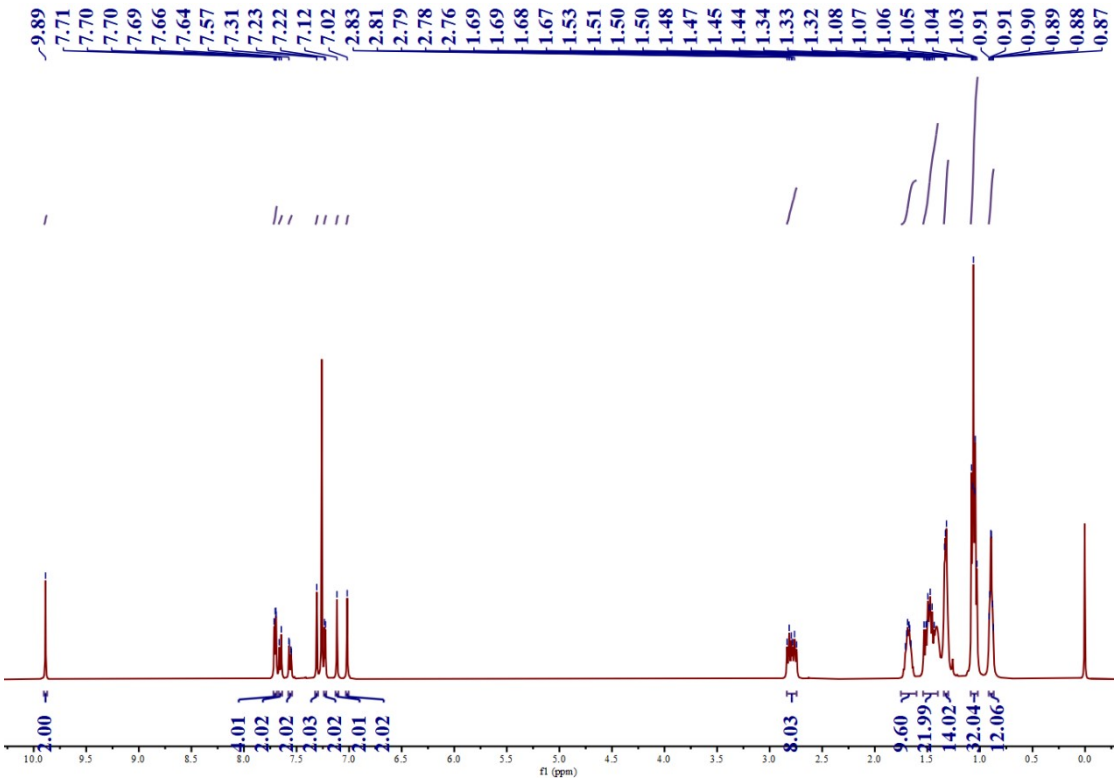

Figure S12. ^{1}H NMR spectrum of compound 2b in $CDCl_3$.

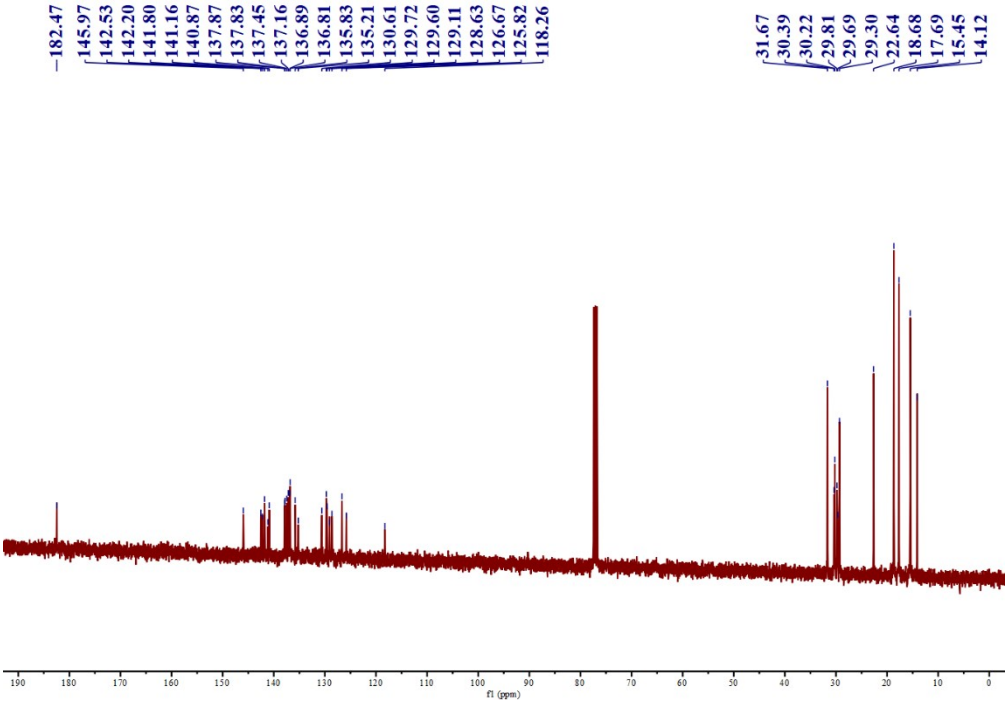

Figure S13. ^{13}C NMR spectrum of compound 2b in $CDCl_3$.

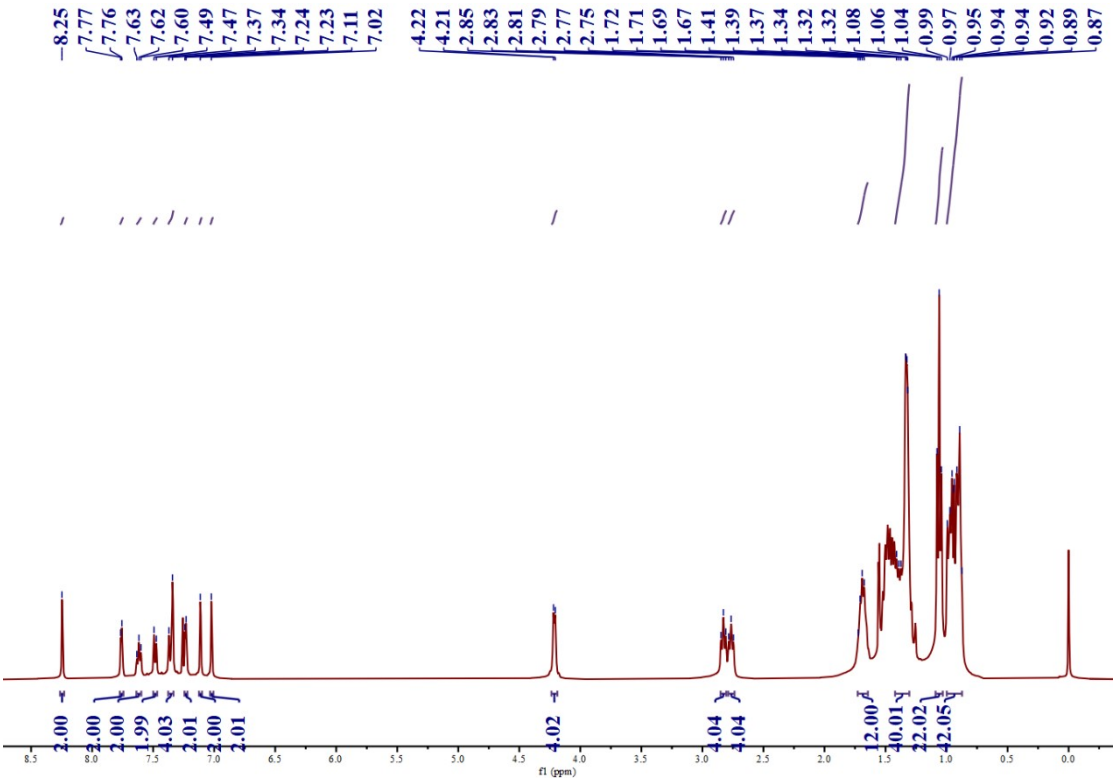

Figure S14. ^{1}H NMR spectrum of compound T25 in $CDCl_3$.

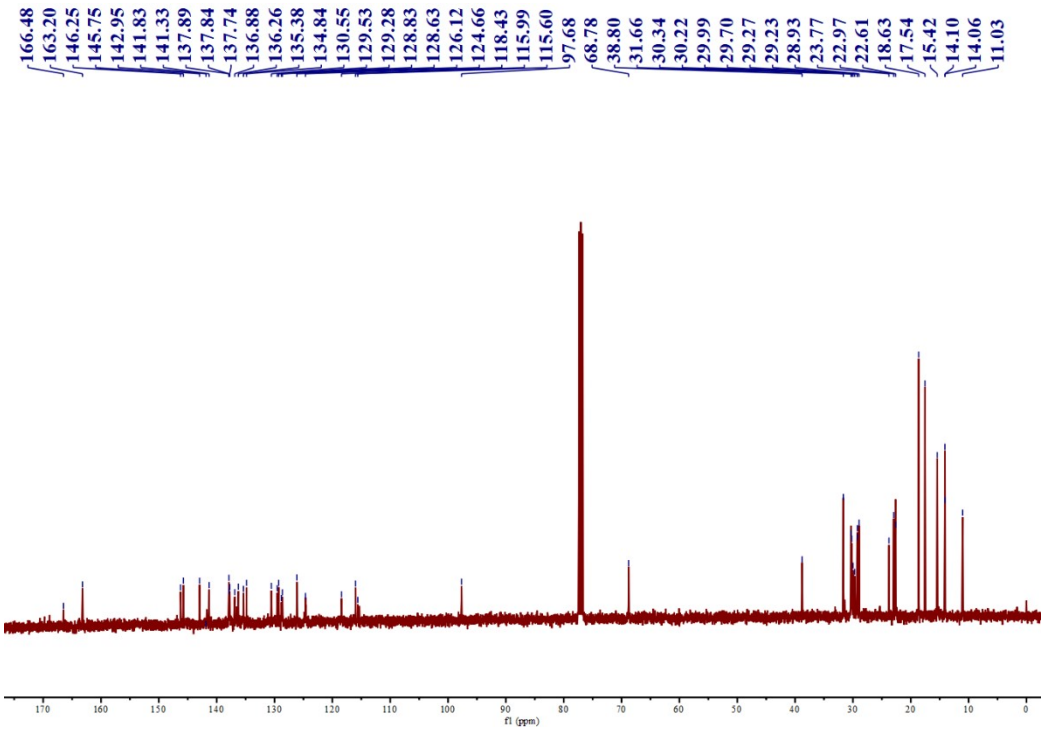

Figure S15. ^{13}C NMR spectrum of compound T25 in $CDCl_3$.

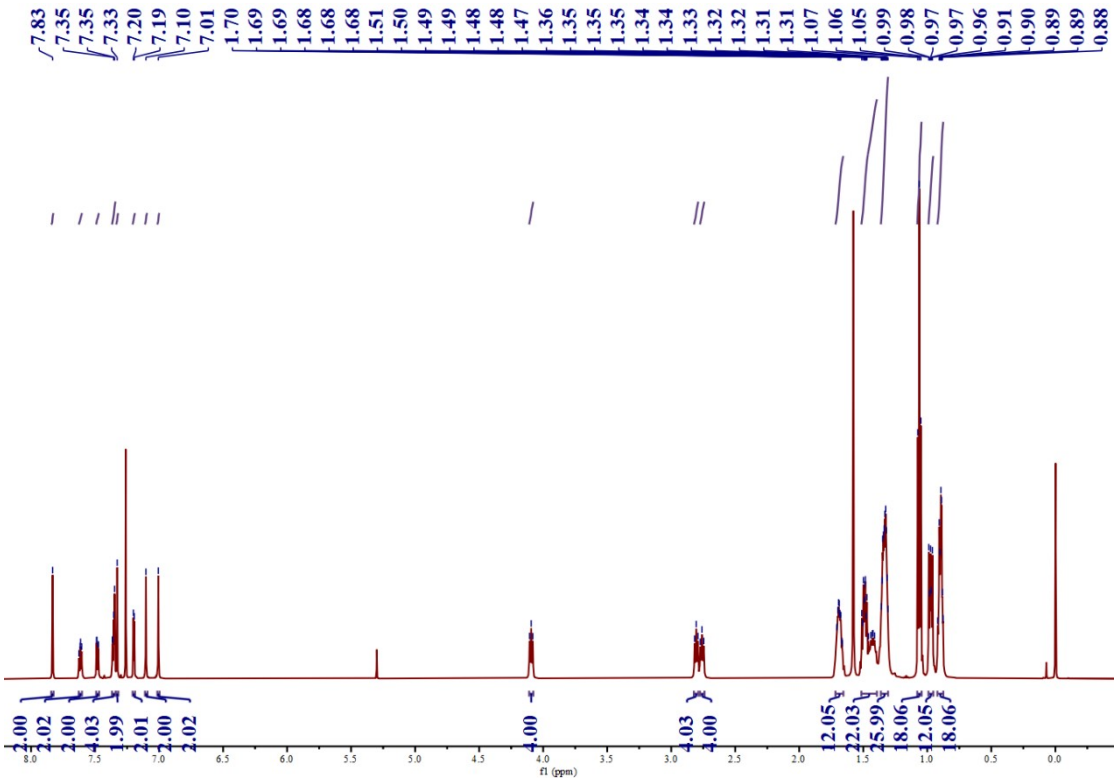

Figure S16. ^{1}H NMR spectrum of compound T26 in $CDCl_3$

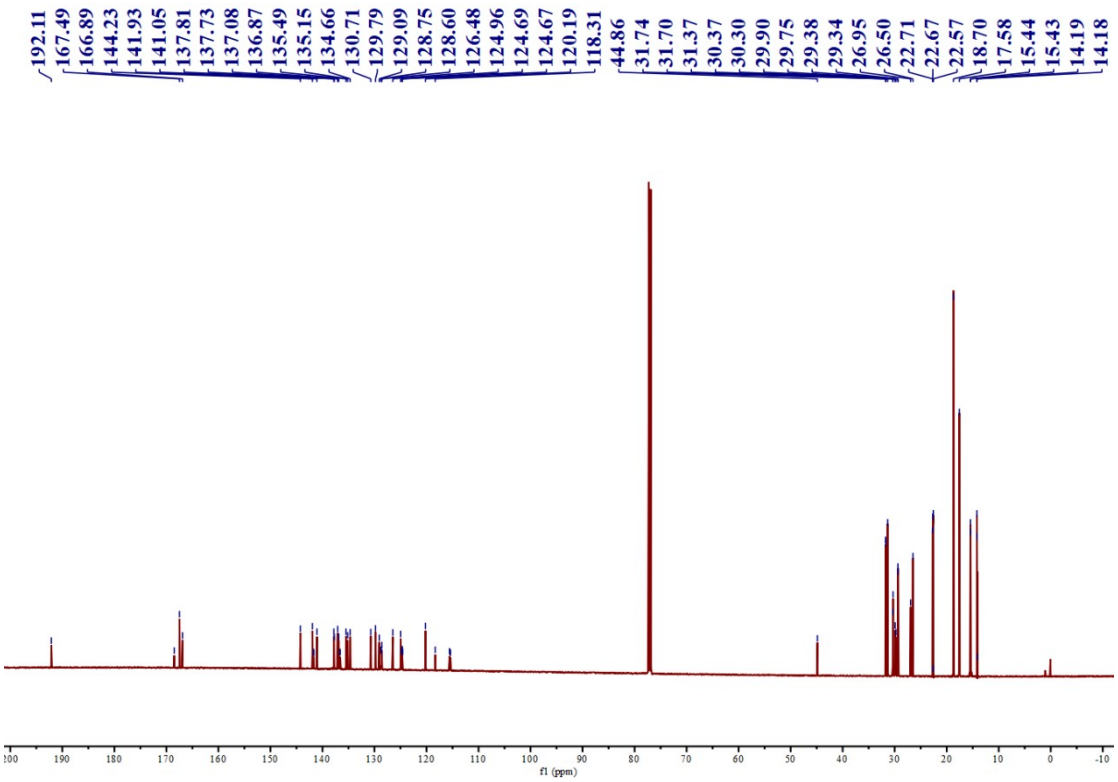

Figure S17. ^{13}C NMR spectrum of compound T26 in $CDCl_3$.

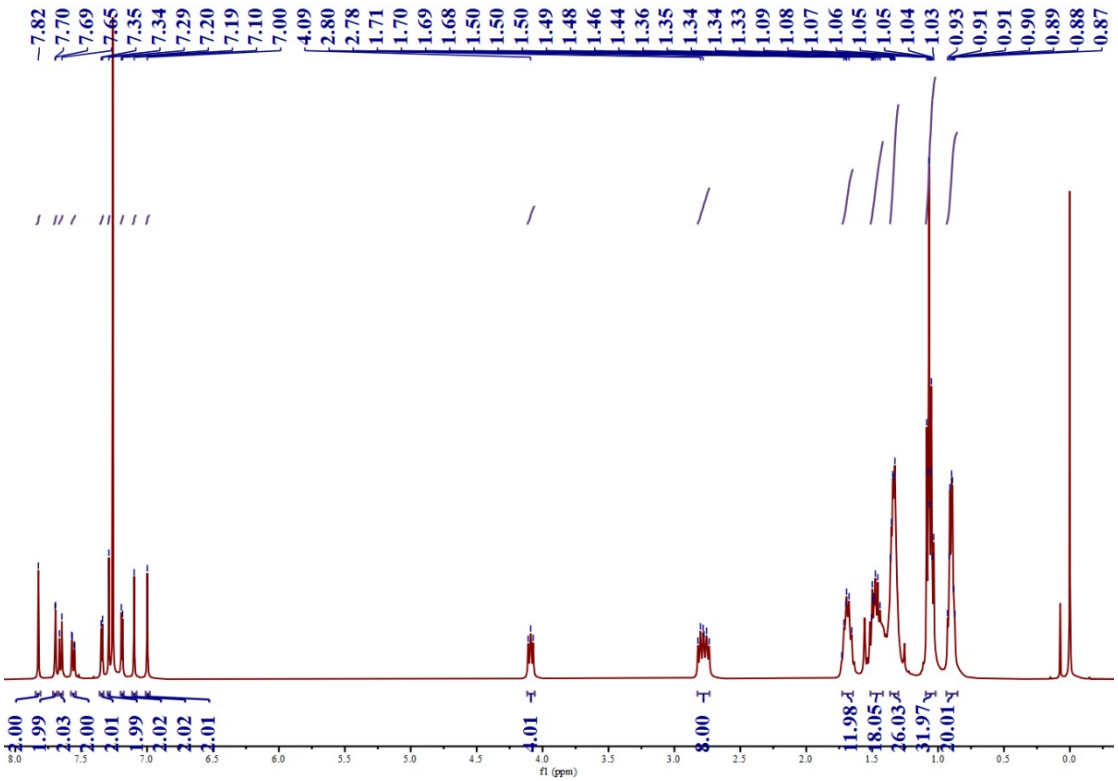

Figure S18. ^{1}H NMR spectrum of compound T27 in $CDCl_3$

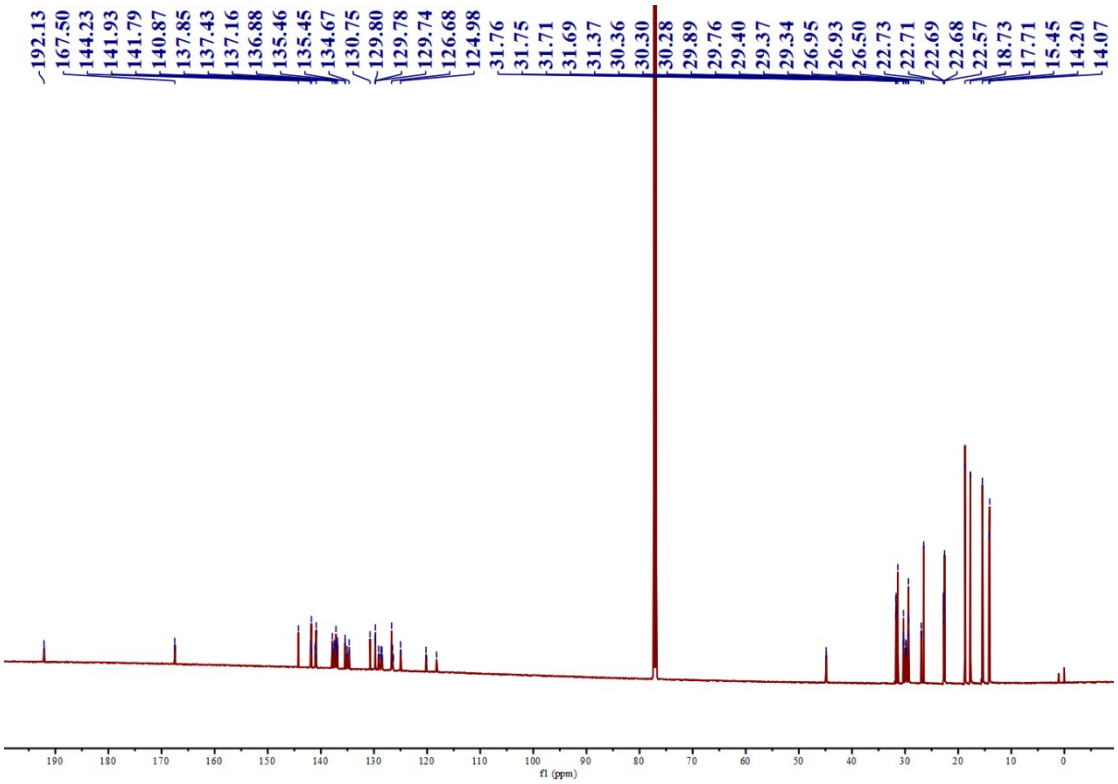

Figure S19. ^{13}C NMR spectrum of compound T27 in $CDCl_3$.

Table S1. The values of the four-point energy and internal reorganization energy of the three SMDs.

basename		T25	T26	T27
scf(a.u.)	CN	-6918.91823492	-8360.91910406	-9081.52558158
	CC	-6918.70369599	-8360.70646382	-9081.31261343
	NC	-6918.70145218	-8360.70466270	-9081.31082215
	NN	-6918.92166636	-8360.92233042	-9081.52879332
λ_{INT} (meV)		154.43	136.80	136.14

Table S2. Photovoltaic data of T27:Y6 solar cells with 1.5:1 ratio under different posttreatment condition. All data were obtained under illumination of AM 1.5G (100mW cm^{-2}) light source.

Condition	Voc (V)	PCE_{max} (%)	FF (%)	Jsc (mA/cm^2)
100°C, 10min	0.906	6.25	37.66	18.30
110°C, 10min	0.887	8.53	44.04	21.83
120°C, 10min	0.869	9.86	48.28	23.50
130°C, 10min	0.843	9.81	48.73	23.85

Table S3. Blend film thickness dependence for T27:Y6 solar cells with 1.5:1 ratio under 100°C, 10min. All data were obtained under illumination of AM 1.5G (100mW cm^{-2}) light source.

Speed (rpm)	Voc (V)	PCE_{max} (%)	FF (%)	Jsc (mA/cm^2)
2000	0.895	5.88	36.14	18.19
2500	0.905	6.37	38.18	18.39
3000	0.902	6.01	36.83	18.09

Table S4. Photovoltaic data of T27:Y6 solar cells with different solvent vapor annealing. All data were obtained under illumination of AM 1.5G (100mW cm^{-2}) light source.

D:A	condition	Voc (V)	PCE_{max} (%)	FF (%)	Jsc (mA/cm^2)
1.5:1	CS_2,40s	0.883	12.00	57.52	23.65
	CF,40s	0.848	12.03	61.00	23.24
	CB,50s	0.846	14.99	68.82	25.72
	120°C, 5min, CS_2,40s	0.883	11.86	55.30	24.28
	120°C, 5min, CF,40s	0.869	11.38	53.78	24.35
	120°C, 5min, CB,50s	0.859	13.68	62.56	25.47

Table S5. Photovoltaic data of T27:Y6 solar cells with different solvent vapor annealing. All data were obtained under illumination of AM 1.5G (100mW cm^{-2}) light source.

D:A	condition	Voc (V)	PCE_{max} (%)	FF (%)	Jsc (mA/cm^2)
1.5:1	CB,40S,120,2min	0.877	13.21	57.06	26.40
	CB,50S,120,2min	0.845	15.06	67.46	26.42
	CS2,40S,120,2min	0.871	14.74	63.60	26.62
	CS2,50S,120,2min	0.874	14.61	63.50	26.31
	THF,40S,120,2min	0.857	13.60	60.53	26.21
	THF,50S,120,2min	0.860	13.70	59.75	26.67
	DCM,40S,120,2min	0.881	11.79	52.75	25.39
	DCM,50S,120,2min	0.878	12.07	53.68	25.62

Table S6. Photovoltaic data of T27:Y6 solar cells with different solvent vapor annealing time. All data were obtained under illumination of AM 1.5G (100mW cm^{-2}) light source

D:A	condition	Voc (V)	PCE_{max} (%)	FF (%)	Jsc (mA/cm^2)
1.5:1	CB,50s,120,2min	0.844	15.92	70.79	26.65
	CB,60s,120,2min	0.841	16.50	72.81	26.94
	CB,70s,120,2min	0.834	15.17	69.85	26.01

Table S7. Donor-Acceptor ratio dependence for T27:Y6 devices with the same conditions.

[A] Ratio	Voc (V)	PCE_{max} (%)	FF (%)	Jsc (mA/cm^2)
1.3:1	0.833	15.40	71.10	25.99
1.4:1	0.833	16.01	72.05	26.68
1.5:1	0.838	16.77	74.38	26.89
1.6:1	0.835	16.41	73.43	26.75
1.7:1	0.837	16.07	70.65	26.71

Table S8. Photovoltaic parameters of thick-film all-small molecules with different active layer thickness.

Active layer	Thickness [nm]	J_{sc} [mA cm^{-2}]	V_{oc} [V]	FF [%]	PCE[%]	Ref.
DR3TSBDT:$PC_{71}BM$	280	15.82	0.88	65.3	9.05	3
BTR: $PC_{71}BM$	310	14.5	0.94	70	9.5	4
BTR:NITI: $PC_{71}BM$	300	19.5	0.94	73.83	13.63	5
BTR:BTR-OH: $PC_{71}BM$	300	14.62	0.93	74.2	10.14	6
SM1-F:Y6	250	21.9	0.85	64	11.9	7
L2:Y6	300	24.5	0.82	71.2	14.3	8
HD-1:BYP-eC9	350	27.25	0.811	67.52	14.92	9
This Work	300	27.21	0.812	68.02	15.03	

Table S9. In-plane (IP) and out-of-plane (OOP) parameters extracted from the 2D GIWAXS of pristine films.

Position / Sample	Out-of-plane								In plane											
	010				h00				h00				010				001			
	q(Å^{-1})	d-spacing (Å)	FWHM (Å^{-1})	Coherence length (Å)	q(Å^{-1})	d-spacing (Å)	FWHM (Å^{-1})	Coherence length (Å)	q(Å^{-1})	d-spacing (Å)	FWHM (Å^{-1})	Coherence length (Å)	q(Å^{-1})	d-spacing (Å)	FWHM (Å^{-1})	Coherence length (Å)	q(Å^{-1})	d-spacing (Å)	FWHM (Å^{-1})	Coherence length (Å)
T27	N/A	N/A	N/A	N/A	0.318 (100)	19.8	0.037	151.9	0.393	16.0	0.033	170.1	1.778	3.5	0.317	18.0	N/A	N/A	N/A	N/A
					0.615 (200)	10.2	0.136	41.7												
					0.912 (300)	6.9	0.248	22.9												
T26	N/A	N/A	N/A	N/A	0.318 (100)	19.8	0.039	145.6	0.371	16.9	0.023	242.7	1.718	3.7	0.231	24.7	N/A	N/A	N/A	N/A
					0.639 (200)	9.8	0.068	83.1												
					0.882 (300)	7.1	0.146	38.8												
T25	1.527	4.1	0.289	19.7	0.272 (100)	23.1	0.025	224.3	0.371	16.9	0.023	246.9	1.728	3.6	0.215	26.6	N/A	N/A	N/A	N/A
					0.562 (200)	11.2	0.037	154.3												
					0.839 (300)	7.5	0.053	106.9												
Y6	1.764	3.6	0.244	23.4	N/A	N/A	N/A	N/A	0.357	17.6	0.130	43.5	N/A	N/A	N/A	N/A	0.486	12.9	0.133	42.5

Table S10. In-plane (IP) and out-of-plane (OOP) parameters extracted from the 2D GIWAXS of as cast blend films.

Position / Sample	Out-of-plane								In plane							
	010				100				100				010			
	q(Å^{-1})	d-spacing (Å)	FWHM (Å^{-1})	Coherence length (Å)	q(Å^{-1})	d-spacing (Å)	FWHM (Å^{-1})	Coherence length (Å)	q(Å^{-1})	d-spacing (Å)	FWHM (Å^{-1})	Coherence length (Å)	q(Å^{-1})	d-spacing (Å)	FWHM (Å^{-1})	Coherence length (Å)
T27:Y6	1.697	3.7	0.174	32.9	N/A	N/A	N/A	N/A	0.433	14.5	0.043	131.5	N/A	N/A	N/A	N/A
T26:Y6	1.633	3.8	0.203	28.1	0.275	22.9	0.053	106.3	0.349	18.0	0.035	160.4	N/A	N/A	N/A	N/A
T25:Y6	1.633	3.8	0.191	30.0	0.278	22.6	0.067	84.1	0.351	17.9	0.034	164.7	N/A	N/A	N/A	N/A

Table S11. The calculated C and S concentration in acceptor and donor.

Elements	Donor			Acceptor
	T25	T26	T27	Y6
C	0.73	0.69	0.67	0.48
S	0.052	0.076	0.075	0.029

Reference

1. Xu, T. *et al*. Deciphering the Role of Side-Chain Engineering and Solvent Vapor Annealing for Binary All-Small-Molecule Organic Solar Cells. *Adv. Funct. Mater*. **33**, 2210549 (2022).

2. Xu, W. *et al*. Improved photovoltaic properties of copolymer donors by regulating

alkyl and alkylsilyl side chains. Dyes and Pigments **197**, 109842 (2022).

3. Zhang, Q. *et al*. Large active layer thickness toleration of high-efficiency small molecule solar cells. *J. Mater. Chem. A* **3**, 22274-22279 (2015).

4. Armin, A. *et al*. Reduced Recombination in High Efficiency Molecular Nematic Liquid Crystalline: Fullerene Solar Cells. *Adv. Energy Mater*. **6**, 1600939 (2016).

5. Zhou, Z. *et al*. High-efficiency small-molecule ternary solar cells with a hierarchical morphology enabled by synergizing fullerene and non-fullerene acceptors. *Nat. Energy* **3**, 952-959 (2018).

6. Tang, H. *et al*. Donor Derivative Incorporation: An Effective Strategy toward High Performance All-Small-Molecule Ternary Organic Solar Cells. *Adv. Sci.* (Weinh) **6**, 1901613 (2019).

7. Qiu, B. *et al*. Highly Efficient All-Small-Molecule Organic Solar Cells with Appropriate Active Layer Morphology by Side Chain Engineering of Donor Molecules and Thermal Annealing. *Adv. Mater.* **32**, e1908373 (2020).

8. Xu, T. *et al*. 15.8% efficiency binary all-small-molecule organic solar cells enabled by a selenophene substituted sematic liquid crystalline donor. *Energy & Environ. Sci.* **14**, 5366-5376 (2021).

9. Ma, K. *et al.* Modulation of Alkyl Chain Length on the Thiazole Side Group Enables Over 17% Efficiency in All-Small-Molecule Organic Solar Cells. *Adv.Funct. Mater*. **33**, 2214926 (2023).